
Bilinear Attention Networks

Jin-Hwa Kim¹ Jaehyun Jun¹ Byoung-Tak Zhang^{1,2}

¹Seoul National University, ²Surromind Robotics

{jhhkim, jhjun, btzhang}@bi.snu.ac.kr

Abstract

Attention networks in multimodal learning provide an efficient way to utilize given visual information selectively. However, the computational cost to learn attention distributions for every pair of multimodal input channels is prohibitively expensive. To solve this problem, co-attention builds two separate attention distributions for each modality neglecting the interaction between multimodal inputs. In this paper, we propose bilinear attention networks (BAN) that find bilinear attention distributions to utilize given vision-language information seamlessly. BAN considers bilinear interactions among two groups of input channels, while low-rank bilinear pooling extracts the joint representations for each pair of channels. Furthermore, we propose a variant of multimodal residual networks to exploit eight-attention maps of the BAN efficiently. We quantitatively and qualitatively evaluate our model on visual question answering (VQA 2.0) and Flickr30k Entities datasets, showing that BAN significantly outperforms previous methods and achieves new state-of-the-arts on both datasets.

1 Introduction

Machine learning for computer vision and natural language processing accelerates the advancement of artificial intelligence. Since vision and natural language are the major modalities of human interaction, understanding and reasoning of vision and natural language information become a key challenge. For instance, visual question answering involves a vision-language cross-grounding problem. A machine is expected to answer given questions like "who is wearing glasses?", "is the umbrella upside down?", or "how many children are in the bed?" exploiting visually-grounded information.

For this reason, visual attention based models have succeeded in multimodal learning tasks, identifying selective regions in a spatial map of an image defined by the model. Also, textual attention can be considered along with visual attention. The attention mechanism of co-attention networks [35, 18, 20, 38] concurrently infers visual and textual attention distributions for each modality. The co-attention networks selectively attend to question words in addition to a part of image regions. However, the co-attention neglects the interaction between words and visual regions to avoid increasing computational complexity.

In this paper, we extend the idea of co-attention into bilinear attention which considers every pair of multimodal channels, *e.g.*, the pairs of question words and image regions. If the given question involves multiple visual concepts represented by multiple words, the inference using visual attention distributions for each word can exploit relevant information better than that using single compressed attention distribution.

From this background, we propose bilinear attention networks (BAN) to use a bilinear attention distribution, on top of low-rank bilinear pooling [15]. Notice that the BAN exploits bilinear interactions between two groups of input channels, while low-rank bilinear pooling extracts the joint representations for each pair of channels. Furthermore, we propose a variant of multimodal residual networks (MRN) to efficiently utilize the multiple bilinear attention maps of the BAN, unlike the

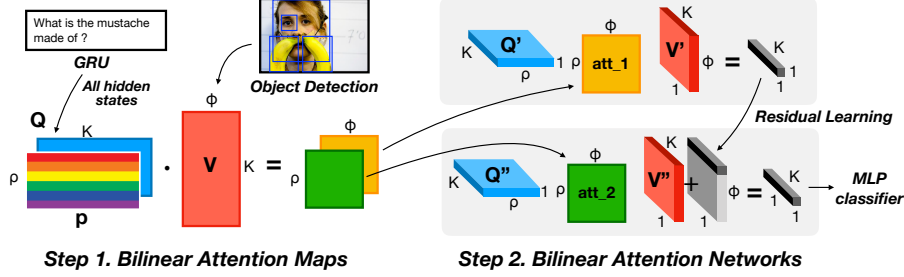


Figure 1: Overview of a two-layer BAN. Two multi-channel inputs, ϕ -object detection features and ρ -length GRU hidden vectors, are used to get bilinear attention maps and joint representations to be used by a classifier. For the definition of the BAN, see the text in Section 3.

previous works [6, 15] where multiple attention maps are used by concatenating the attended features. Since the proposed residual learning method for BAN exploits residual summations instead of concatenation, which leads to parameter-efficiently and performance-effectively learn up to eight-glimpse BAN. For the overview of two-glimpse BAN, please refer to Figure 1.

Our main contributions are:

- We propose the bilinear attention networks (BAN) to learn and use bilinear attention distributions, on top of low-rank bilinear pooling technique.
- We propose a variant of multimodal residual networks (MRN) to efficiently utilize the multiple bilinear attention maps generated by our model. Unlike previous works, our method successfully utilizes up to 8 attention maps.
- Finally, we validate our proposed method on a large and highly-competitive dataset, VQA 2.0 [8]. Our model achieves a new state-of-the-art maintaining simplicity of model structure. Moreover, we evaluate the visual grounding of bilinear attention map on Flickr30k Entities [23] outperforming previous methods, along with 25.37% improvement of inference speed taking advantage of the processing of multi-channel inputs.

2 Low-rank bilinear pooling

We first review the low-rank bilinear pooling and its application to attention networks [15], which uses single-channel input (question vector) to combine the other multi-channel input (image features) as single-channel intermediate representation (attended feature).

Low-rank bilinear model. Pirsiavash et al. [22] proposed a low-rank bilinear model to reduce the rank of bilinear weight matrix \mathbf{W}_i to give regularity. For this, \mathbf{W}_i is replaced with the multiplication of two smaller matrices $\mathbf{U}_i \mathbf{V}_i^T$, where $\mathbf{U}_i \in \mathbb{R}^{N \times d}$ and $\mathbf{V}_i \in \mathbb{R}^{M \times d}$. As a result, this replacement makes the rank of \mathbf{W}_i to be at most $d \leq \min(N, M)$. For the scalar output f_i (bias terms are omitted without loss of generality):

$$f_i = \mathbf{x}^T \mathbf{W}_i \mathbf{y} = \mathbf{x}^T \mathbf{U}_i \mathbf{V}_i^T \mathbf{y} = \mathbf{1}^T (\mathbf{U}_i^T \mathbf{x} \circ \mathbf{V}_i^T \mathbf{y}) \quad (1)$$

where $\mathbf{1} \in \mathbb{R}^d$ is a vector of ones and \circ denotes Hadamard product (element-wise multiplication).

Low-rank bilinear pooling. For a vector output \mathbf{f} , a pooling matrix \mathbf{P} is introduced:

$$\mathbf{f} = \mathbf{P}^T (\mathbf{U}^T \mathbf{x} \circ \mathbf{V}^T \mathbf{y}) \quad (2)$$

where $\mathbf{P} \in \mathbb{R}^{d \times c}$, $\mathbf{U} \in \mathbb{R}^{N \times d}$, and $\mathbf{V} \in \mathbb{R}^{M \times d}$. It allows \mathbf{U} and \mathbf{V} to be two-dimensional tensors by introducing \mathbf{P} for a vector output $\mathbf{f} \in \mathbb{R}^c$, significantly reducing the number of parameters.

Unitary attention networks. Attention provides an efficient mechanism to reduce input channel by selectively utilizing given information. Assuming that a multi-channel input \mathbf{Y} consisting of $\phi = \{y_i\}$ column vectors, we want to get single channel \hat{y} from \mathbf{Y} using the weights $\{\alpha_i\}$:

$$\hat{y} = \sum_i \alpha_i y_i \quad (3)$$

where α represents an attention distribution to selectively combine ϕ input channels. Using the low-rank bilinear pooling, the α is defined by the output of softmax function as:

$$\alpha := \text{softmax}\left(\mathbf{P}^T((\mathbf{U}^T \mathbf{x} \cdot \mathbf{1}^T) \circ (\mathbf{V}^T \mathbf{Y}))\right) \quad (4)$$

where $\alpha \in \mathbb{R}^{G \times \phi}$, $\mathbf{P} \in \mathbb{R}^{d \times G}$, $\mathbf{U} \in \mathbb{R}^{N \times d}$, $\mathbf{x} \in \mathbb{R}^N$, $\mathbf{1} \in \mathbb{R}^\phi$, $\mathbf{V} \in \mathbb{R}^{M \times d}$, and $\mathbf{Y} \in \mathbb{R}^{M \times \phi}$. If $G > 1$, multiple glimpses (*a.k.a.* attention heads) are used [13, 6, 15], then $\hat{\mathbf{y}} = \prod_{g=1}^G \sum_i \alpha_{g,i} \mathbf{y}_i$, the concatenation of attended outputs. Finally, two single channel inputs \mathbf{x} and $\hat{\mathbf{y}}$ can be used to get the joint representation using the other low-rank bilinear pooling for a classifier.

3 Bilinear attention networks

We generalize a bilinear model for two multi-channel inputs, $\mathbf{X} \in \mathbb{R}^{N \times \rho}$ and $\mathbf{Y} \in \mathbb{R}^{M \times \phi}$, where $\rho = |\{\mathbf{x}_i\}|$ and $\phi = |\{\mathbf{y}_j\}|$, the numbers of two input channels, respectively. To reduce both input channel simultaneously, we introduce bilinear attention map $\mathcal{A} \in \mathbb{R}^{\rho \times \phi}$ as follows:

$$\mathbf{f}'_k = (\mathbf{X}^T \mathbf{U}')^T \mathcal{A} (\mathbf{Y}^T \mathbf{V}')_k \quad (5)$$

where $\mathbf{U}' \in \mathbb{R}^{N \times K}$, $\mathbf{V}' \in \mathbb{R}^{M \times K}$, $(\mathbf{X}^T \mathbf{U}')_k \in \mathbb{R}^\rho$, $(\mathbf{Y}^T \mathbf{V}')_k \in \mathbb{R}^\phi$, and \mathbf{f}'_k denotes the k -th element of intermediate representation. The subscript k for the matrices indicates the index of column. Notice that Equation 5 is a bilinear model for the two groups of input channels where \mathcal{A} in the middle is a bilinear weight matrix. Interestingly, Equation 5 can be rewritten as:

$$\mathbf{f}'_k = \sum_{i=1}^{\rho} \sum_{j=1}^{\phi} \mathcal{A}_{i,j} (\mathbf{X}_i^T \mathbf{U}'_k) (\mathbf{V}'_k^T \mathbf{Y}_j) = \sum_{i=1}^{\rho} \sum_{j=1}^{\phi} \mathcal{A}_{i,j} \mathbf{X}_i^T (\mathbf{U}'_k \mathbf{V}'_k^T) \mathbf{Y}_j \quad (6)$$

where \mathbf{X}_i and \mathbf{Y}_j denotes the i -th channel (column) of input \mathbf{X} and the j -th channel (channel) of input \mathbf{Y} , respectively, \mathbf{U}'_k and \mathbf{V}'_k denotes the k -th column of \mathbf{U}' and \mathbf{V}' matrices, respectively, and $\mathcal{A}_{i,j}$ denotes an element in the i -th row and the j -th column of \mathcal{A} . Notice that, for each pair of channels, the 1-rank bilinear representation of two feature vectors is modeled in $\mathbf{X}_i^T (\mathbf{U}'_k \mathbf{V}'_k^T) \mathbf{Y}_j$ of Equation 6 (eventually at most K -rank bilinear pooling for $\mathbf{f}' \in \mathbb{R}^K$). Then, the bilinear joint representation is $\mathbf{f} = \mathbf{P}^T \mathbf{f}'$ where $\mathbf{f} \in \mathbb{R}^C$ and $\mathbf{P} \in \mathbb{R}^{K \times C}$. For the convenience, we define the bilinear attention networks as a function of two multi-channel inputs parameterized by a bilinear attention map as follows:

$$\mathbf{f} = \text{BAN}(\mathbf{X}, \mathbf{Y}; \mathcal{A}). \quad (7)$$

Bilinear attention map. Now, we want to get the attention map similarly to Equation 4. Using Hadamard product and matrix-matrix multiplication, the attention map \mathcal{A} is defined as:

$$\mathcal{A} := \text{softmax}\left(\left((\mathbf{1} \cdot \mathbf{p}^T) \circ \mathbf{X}^T \mathbf{U}\right) \mathbf{V}^T \mathbf{Y}\right) \quad (8)$$

where $\mathbf{1} \in \mathbb{R}^\rho$, $\mathbf{p} \in \mathbb{R}^{K'}$, and remind that $\mathcal{A} \in \mathbb{R}^{\rho \times \phi}$. The softmax function is applied element-wisely. Notice that each logit $A_{i,j}$ of the softmax is the output of low-rank bilinear pooling as:

$$A_{i,j} = \mathbf{p}^T \left((\mathbf{U}^T \mathbf{X}_i) \circ (\mathbf{V}^T \mathbf{Y}_j) \right). \quad (9)$$

The multiple bilinear attention maps can be extended as follows:

$$\mathcal{A}_g := \text{softmax}\left(\left((\mathbf{1} \cdot \mathbf{p}_g^T) \circ \mathbf{X}^T \mathbf{U}\right) \mathbf{V}^T \mathbf{Y}\right) \quad (10)$$

where the parameters of \mathbf{U} and \mathbf{V} are shared, but not for \mathbf{p}_g where g denotes the index of glimpses.

Residual learning of attention. Inspired by multimodal residual networks (MRN) from Kim et al. [14], we propose a variant of MRN to integrate the joint representations from the multiple bilinear attention maps. The $i + 1$ -th output is defined as:

$$\mathbf{f}_{i+1} = \text{BAN}_i(\mathbf{f}_i, \mathbf{Y}; \mathcal{A}_i) \cdot \mathbf{1}^T + \mathbf{f}_i \quad (11)$$

where $\mathbf{f}_0 = \mathbf{X}$ (if $N = K$) and $\mathbf{1} \in \mathbb{R}^\rho$. Here, the size of \mathbf{f}_i is the same with the size of \mathbf{X} as successive attention maps are processed. To get the logits for a classifier, *e.g.*, two-layer MLP, we sum over the channel dimension of the last output \mathbf{f}_G , where G is the number of glimpses.

Time complexity. When we assume that the number of input channels is smaller than feature sizes, $M \geq N \geq K \gg \phi \geq \rho$, the time complexity of the BAN is the same with the case of one multi-channel input as $\mathcal{O}(KM\phi)$ for single glimpse model. Since the BAN consists of matrix chain multiplication and exploits the property of low-rank factorization in the low-rank bilinear pooling.

4 Related works

Multimodal factorized bilinear pooling. Yu et al. [38] extends low-rank bilinear pooling [15] using the rank > 1 . They remove a projection matrix \mathbf{P} , instead, d in Equation 2 is replaced with much smaller k while \mathbf{U} and \mathbf{V} are three-dimensional tensors. However, this generalization was not effective for BAN, at least in our experimental setting. Please see *BAN-I+MFB* in Figure 2b where the performance is not significantly improved from that of *BAN-I*. Furthermore, the peak GPU memory consumption is larger due to its model structure which hinders to use multiple-glimpse BAN.

Co-attention networks. Xu and Saenko [35] proposed the spatial memory network model estimating the correlation among every image patches and tokens in a sentence. The estimated correlation \mathbf{C} is defined as $(\mathbf{UX})^T \mathbf{Y}$ in our notation. Unlike our method, they get an attention distribution $\alpha = \text{softmax}(\max_{i=1, \dots, \rho}(\mathbf{C}_i)) \in \mathbb{R}^\rho$ where the logits to softmax is the maximum values in each row vector of \mathbf{C} . The attention distribution for the other input can be calculated similarly. There are variants of co-attention networks [18, 20], especially, Lu et al. [18] sequentially get two attention distributions conditioning on the other modality. Recently, Yu et al. [38] reduce the co-attention method into two steps, self-attention for a question embedding and the question-conditioned attention for a visual embedding. However, these co-attention approaches use separate attention distributions for each modality, neglecting the interaction between the modalities what we consider and model.

5 Experiments

5.1 Datasets

Visual Question Answering (VQA). We evaluate on the VQA 2.0 dataset [1, 8], which is improved from the previous version to emphasize visual understanding by reducing the answer bias in the dataset. This improvement pushes the model to have more effective joint representation of question and image, which fits the motivation of our bilinear attention approach. The VQA evaluation metric considers inter-human variability defined as $\text{Accuracy}(ans) = \min(\#\text{humans that said } ans/3, 1)$. Note that reporting accuracies are averaged over all ten choose nine sets of ground-truths. The test set is split into test-dev, test-standard, test-challenge, and test-reserve. The annotations for the test set are unavailable except the remote evaluation servers.

Flickr30k Entities. For the evaluation of visual grounding by the bilinear attention maps, we use Flickr30k Entities [23] consisting of 31,783 images [37] and 244,035 annotations that multiple entities (phrases) in a sentence for an image are mapped to the boxes on the image to indicate the correspondences between them. The task is to localize a corresponding box for each entity. In this way, visual grounding of textual information is quantitatively measured. Following the evaluation metric [23], if a predicted box has the intersection over union (IoU) of overlapping area with one of the ground-truth boxes which are greater than or equal to 0.5, the prediction for a given entity is correct. This metric is called Recall@1. If K predictions are permitted to find at least one correction, it is called Recall@K. We report Recall@1, 5, and 10 to compare state-of-the-arts (R@K in Table 4). The upper bound of performance depends on the performance of object detection if the detector proposes candidate boxes for the prediction.

5.2 Preprocessing

Question embedding. For VQA, we get a question embedding $\mathbf{X}^T \in \mathbb{R}^{14 \times N}$ using GloVe word embeddings [21] and the outputs of Gated Recurrent Unit (GRU) [5] for every time-steps up to the first 14 tokens following the previous work [29]. The questions shorter than 14 words are end-padded with zero vectors. For Flickr30k Entities, we use a full length of sentences (82 is maximum) to get all entities. We mark the token positions which are at the end of each annotated phrase. Then, we select a subset of the output channels of GRU using these positions, which makes the number of channels is the number of entities in a sentence. The word embeddings and GRU are fine-tuned in training.

Image features. We use the image features extracted from bottom-up attention [2]. These features are the output of Faster R-CNN [25], pre-trained using Visual Genome [17]. We set a threshold for object detection to get $\phi = 10$ to 100 objects per image. The features are represented as $\mathbf{Y}^T \in \mathbb{R}^{\phi \times 2,048}$, which is fixed while training. To deal with variable-channel inputs, we mask the padding logits with minus infinite to get zero probability from softmax avoiding underflow.

5.3 Nonlinearity and classifier

Nonlinearity. We use ReLU [19] to give nonlinearity to BAN as $\mathbf{f}'_k = \sigma(\mathbf{X}^T \mathbf{U}')^T_k \cdot \mathcal{A} \cdot \sigma(\mathbf{Y}^T \mathbf{V}')_k$ where σ denotes $\text{ReLU}(x) := \max(x, 0)$. For the attention maps, the logits A_g is defined as $((\mathbf{1} \cdot \mathbf{p}_g^T) \circ \sigma(\mathbf{X}^T \mathbf{U})) \cdot \sigma(\mathbf{V}^T \mathbf{Y})$. Note that $\mathbf{X}^T \mathbf{U}$ and $\mathbf{V}^T \mathbf{Y}$ are corresponding to the question embedding matrix \mathbf{Q} and the detected object features \mathbf{V} in Figure 1, respectively.

Classifier. For VQA, we use a two-layer multi-layer perceptron as a classifier for the final joint representation \mathbf{f}_G . The activation function is ReLU. The number of outputs is determined by the minimum occurrence of the answer in unique questions as nine times in the dataset, which is 3,129. Binary cross entropy is used for the loss function following the previous work [29]. For Flickr30k Entities, we take the output of bilinear attention map, and binary cross entropy is used for this output.

5.4 Hyperparameters and regularization

Hyperparameters. The size of image features and question embeddings are $M = 2,048$ and $N = 1,024$, respectively. The size of joint representation C is the same with the rank K in low-rank bilinear pooling, $C = K = 1,024$, but $K' = K \times 3$ is used in the bilinear attention maps to increase a representational capacity for residual learning of attention. Every linear mapping is regularized by Weight Normalization [27] and Dropout [28] ($p = .2$, except for the classifier with .5). Adamax optimizer [16], a variant of Adam based on infinite norm, is used. The learning rate is $\min(i e^{-3}, 4 e^{-3})$ where i is the number of epochs starting from 1, then after 10 epochs, the learning rate is decayed by 1/4 for every 2 epochs up to 13 epochs (*i.e.* $1 e^{-3}$ for 11-th and $2.5 e^{-4}$ for 13-th epoch). We clip the 2-norm of vectorized gradients to .25. The batch size is 512.

Regularization. For the test split of VQA, both train and validation splits are used for training. We augment a subset of Visual Genome [17] dataset following the procedure of the previous works [29]. Accordingly, we adjust the model capacity by increasing all of N , C , and K to 1,280. And, $G = 8$ glimpses are used. For Flickr30k Entities, we use the same test split of the previous methods [23], without additional hyperparameter tuning from VQA experiments.

6 VQA results and discussions

6.1 Quantitative results

Comparison with state-of-the-arts. The first row in Table 1 shows 2017 VQA Challenge winner architecture [2, 29]. BAN significantly outperforms this baseline and successfully utilize up to eight bilinear attention maps to improve its performance taking advantage of residual learning of attention. As shown in Table 3, BAN outperforms the latest model [38] which uses the same bottom-up attention feature [2] by a substantial margin. *BAN-Glove* uses the concatenation of 300-dimensional Glove word embeddings and the semantically-closed mixture of these embeddings (see Appendix A.1). Notice that similar approaches can be found in the competitive models [6, 38] in Table 3 with a different initialization strategy for the same 600-dimensional word embedding. *BAN-Glove-Counter* uses both the previous 600-dimensional word embeddings and counting module [40], which exploits spatial information of detected object boxes from the feature extractor [2]. The learned representation $\mathbf{c} \in \mathbb{R}^{\phi+1}$ for the counting mechanism is linearly projected and added to joint representation after applying ReLU (see Equation 13 in Appendix A.2). In Table 5 (Appendix), we compare with the entries in the leaderboard of both VQA Challenge 2017 and 2018 achieving the 1st place at the time of submission (our entry is not shown in the leaderboard since challenge entries are not visible).

Comparison with other attention methods. *Unitary attention* has a similar architecture with Kim et al. [15] where a question embedding vector is used to calculate the attentional weights for multiple image features of an image. *Co-attention* has the same mechanism of Yu et al. [38], similar to Lu et al. [18], Xu and Saenko [35], where multiple question embeddings are combined as single embedding vector using a self-attention mechanism, then unitary visual attention is applied. Table 2 confirms that bilinear attention is significantly better than any other attention methods. The co-attention is slightly better than simple unitary attention. In Figure 2a, co-attention suffers overfitting more severely (green) than any other methods, while bilinear attention (blue) is more regularized compared with the others. In Figure 2b, BAN is the most parameter-efficient among various attention methods. Notice that four-glimpse BAN more parsimoniously utilizes its parameters than one-glimpse BAN does.

Table 1: Validation scores on VQA 2.0 dataset for the number of glimpses of the BAN. The standard deviations are reported after \pm using three random initialization.

Model	VQA Score
Bottom-Up [29]	63.37 \pm 0.21
BAN-1	65.36 \pm 0.14
BAN-2	65.61 \pm 0.10
BAN-4	65.81 \pm 0.09
BAN-8	66.00 \pm0.11
BAN-12	66.04 \pm0.08

Table 2: Validation scores on VQA 2.0 dataset for attention and integration mechanisms. The $nParams$ indicates the number of parameters. Note that the hidden sizes of unitary attention and co-attention are 1,280, while 1,024 for the BAN.

Model	nParams	VQA Score
Unitary attention	31.9M	64.59 \pm 0.04
Co-attention	32.5M	64.79 \pm 0.06
Bilinear attention	32.2M	65.36 \pm0.14
BAN-4 (residual)	44.8M	65.81 \pm0.09
BAN-4 (sum)	44.8M	64.78 \pm 0.08
BAN-4 (concat)	51.1M	64.71 \pm 0.21

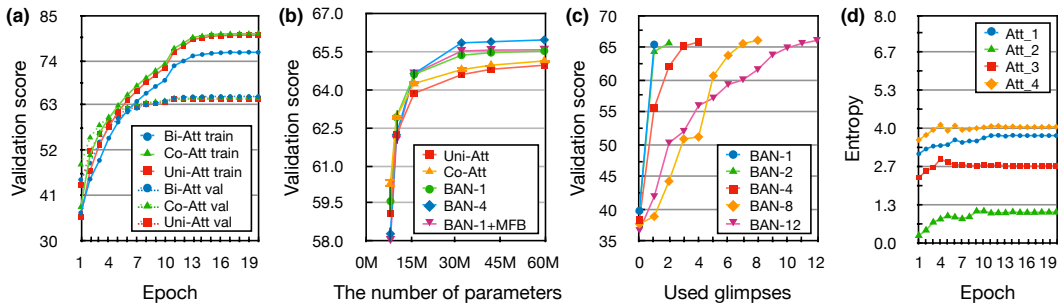


Figure 2: (a) learning curves. Bilinear attention (bi-att) is more robust to overfitting than unitary attention (uni-att) and co-attention (co-att). (b) validation scores for the number of parameters. The error bar indicates the standard deviation among three random initialized models, although it is too small to be noticed for over-15M parameters. (c) ablation study for the first- N -glimpses (x -axis) used in evaluation. (d) the information entropy (y -axis) for each attention map in four-glimpse BAN. The entropy of multiple attention maps is converged to certain levels.

6.2 Residual learning of attention

Comparison with other approaches. In the second section of Table 2, the residual learning of attention significantly outperforms the other methods, *sum*, *i.e.*, $f_G = \sum_i \text{BAN}_i(\mathbf{X}, \mathbf{Y}; \mathcal{A}_i)$, and *concatenation (concat)*, *i.e.*, $f_G = \parallel_i \text{BAN}_i(\mathbf{X}, \mathbf{Y}; \mathcal{A}_i)$. Whereas, the difference between *sum* and *concat* is not significantly different. Notice that the number of parameters of *concat* is larger than the others, since the input size of the classifier is increased.

Ablation study. An interesting property of residual learning is robustness toward arbitrary ablations [31]. To see the relative contributions, we observe the learning curve of validation scores when incremental ablation is performed. First, we train $\{1,2,4,8,12\}$ -glimpse models using training split. Then, we evaluate the model on validation split using the first N attention maps. Hence, the intermediate representation f_N is directly fed into the classifier instead of f_G . As shown in Figure 2c, the accuracy gain of the first glimpse is the highest, then the gain is smoothly decreased as the number of used glimpses is increased.

Entropy of attention. We analyze the information entropy of attention distributions in a four-glimpse BAN. As shown in Figure 2d, the mean entropy of each attention for validation split is converged to a different level of values. This result is repeatably observed in the other number of glimpse models. Our speculation is the multi-attention maps do not equally contribute similarly to voting by committees, but the residual learning by the multi-step attention. We argue that this is a novel observation where the residual learning [9] is used for stacked attention networks.

6.3 Qualitative analysis

The visualization for a two-glimpse BAN is shown in Figure 3. The question is “what color are the pants of the guy skateboarding”. The question and content words, *what*, *pants*, *guy*, and *skateboarding*

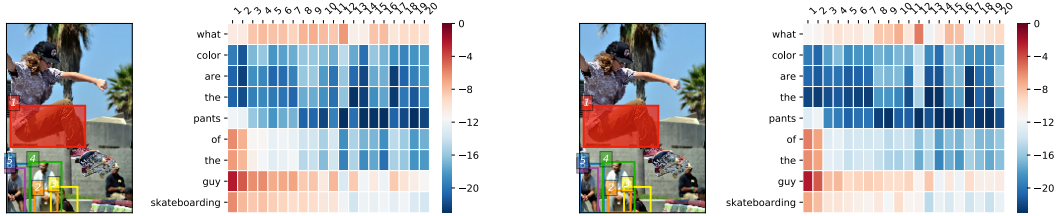


Figure 3: Visualization of the bilinear attention maps for two-glimpse BAN. The left and right groups indicate the first and second bilinear attention maps (right in each group, log-scaled) and the visualized image (left in each group). The most salient six boxes (1-6 numbered in the images and x-axis of the grids) in the first attention map determined by marginalization are visualized on both images to compare. The model gives the correct answer, *brown*.

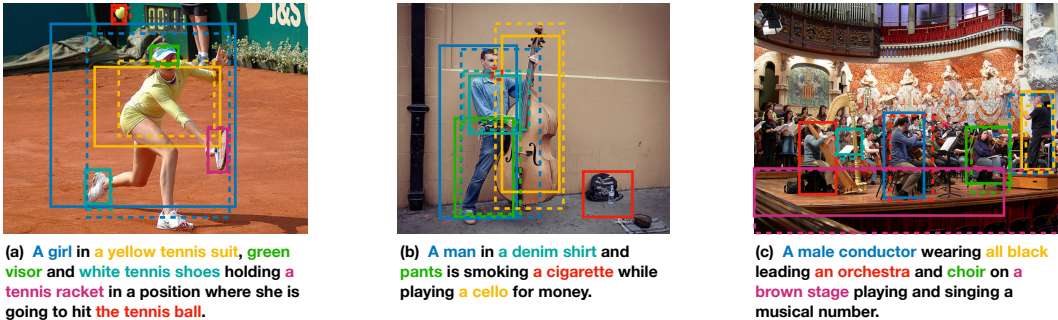


Figure 4: Visualization examples from the test split of Flickr30k Entities are shown. Solid-lined boxes indicate predicted phrase localizations and dashed-line boxes indicate the ground-truth. If there are multiple ground-truth boxes, the closest box is shown to investigate. Each color of a phrase is matched with the corresponding color of predicted and ground-truth boxes. Best view in color.

and skateboarder’s pants in the image are attended. Notice that the box 2 (orange) captured the sitting man’s pants in the bottom.

7 Flickr30k entities results and discussions

To examine the capability of bilinear attention map to capture vision-language interactions, we conduct experiments on Flickr30k Entities [23]. Our experiments show that BAN outperforms the previous state-of-the-art on the phrase localization task with a large margin of 4.48% at a high speed of inference.

Performance. In Table 4, we compare with other previous approaches. Our bilinear attention map to predict the boxes for the phrase entities in a sentence achieves new state-of-the-art with 69.69% for Recall@1. This result is remarkable considering that BAN does not use any additional features like box size, color, segmentation, or pose-estimation [23, 36]. Note that both Query-Adaptive RCNN [10] and our off-the-shelf object detector [2] are based on Faster RCNN [25] and pre-trained on Visual Genome [17]. Compared to Query-Adaptive RCNN, the parameters of our object detector are fixed and only used to extract 10-100 visual features and the corresponding box proposals.

Type. In Table 6 (included in Appendix), we report the results for each type of Flickr30k Entities. Notice that *clothing* and *body parts* are significantly improved to 74.95% and 47.23%, respectively.

Speed. The faster inference is achieved taking advantage of multi-channel inputs in our BAN. Unlike previous methods, BAN is able to infer multiple entities in a sentence which can be prepared as a multi-channel input. Therefore, the number of forwardings to infer is significantly decreased. In our experiment, BAN takes 0.67 ms/entity whereas the setting that single entity as an example takes 0.84 ms/entity, achieving 25.37% improvement. We emphasize that this property is a novel in our model that considers every interaction among vision-language multi-channel inputs.

Table 3: Test-dev and test-standard scores of single-model on VQA 2.0 dataset to compare state-of-the-arts, trained on training and validation splits, and Visual Genome for feature extraction or data augmentation. † This model can be found in <https://github.com/yuzcccc/vqa-mf>, which is not published in a paper.

Model	Overall	Yes/no	Number	Other	Test-std
Bottom-Up [2, 29]	65.32	81.82	44.21	56.05	65.67
MFH [38]	66.12	-	-	-	-
Counter [40]	68.09	83.14	51.62	58.97	68.41
MFH+Bottom-Up [38]†	68.76	84.27	49.56	59.89	-
BAN (ours)	69.52	85.31	50.93	60.26	-
BAN+Glove (ours)	69.66	85.46	50.66	60.50	-
BAN+Glove+Counter (ours)	70.04	85.42	54.04	60.52	70.35

Table 4: Test split results for Flickr30k Entities. We report the average performance of our three randomly-initialized models (the standard deviation of R@1 is 0.17). *Upper Bound* of performance asserted by object detector is shown. † box size and color information are used as additional features. ‡ semantic segmentation, object detection, and pose-estimation is used as additional features. Notice that the detectors of Hinami and Satoh [10] and ours [2] are based on Faster RCNN [25], pre-trained using Visual Genome dataset [17].

Model	Detector	R@1	R@5	R@10	Upper Bound
Zhang et al. [39]	MCG [3]	28.5	52.7	61.3	-
Hu et al. [11]	Edge Boxes [41]	27.8	-	62.9	76.9
Rohrbach et al. [26]	Fast RCNN [7]	42.43	-	-	77.90
Wang et al. [33]	Fast RCNN [7]	42.08	-	-	76.91
Wang et al. [32]	Fast RCNN [7]	43.89	64.46	68.66	76.91
Rohrbach et al. [26]	Fast RCNN [7]	48.38	-	-	77.90
Fukui et al. [6]	Fast RCNN [7]	48.69	-	-	-
Plummer et al. [23]	Fast RCNN [7]†	50.89	71.09	75.73	85.12
Yeh et al. [36]	YOLOv2 [24]‡	53.97	-	-	-
Hinami and Satoh [10]	Query-Adaptive RCNN [10]	65.21	-	-	-
BAN (ours)	Bottom-Up [2]	69.69	84.22	86.35	87.45

Visualization. Figure 4 shows three examples from the test split of Flickr30k Entities. The entities which has visual properties, for instance, *a yellow tennis suit* and *white tennis shoes* in Figure 4a, and *a denim shirt* in Figure 4b, are correct. However, relatively small object (*e.g.*, *a cigarette* in Figure 4b) and the entity that requires semantic inference (*e.g.*, *a male conductor* in Figure 4c) are incorrect.

8 Conclusions

BAN gracefully extends unitary attention networks exploiting bilinear attention maps, where the joint representations of multimodal multi-channel inputs are extracted using low-rank bilinear pooling. Although BAN considers every pair of multimodal input channels, the computational cost remains in the same magnitude, since BAN consists of matrix chain multiplication for efficient computation. The proposed residual learning of attention efficiently uses up to eight bilinear attention maps, keeping the size of intermediate features constant. We believe our BAN gives a new opportunity to learn the richer joint representation for multimodal multi-channel inputs, which appear in many real-world problems.

References

- [1] Aishwarya Agrawal, Jiasen Lu, Stanislaw Antol, Margaret Mitchell, C Lawrence Zitnick, Devi Parikh, and Dhruv Batra. Vqa: Visual question answering. *International Journal of Computer Vision*, 123(1):4–31, 2017.
- [2] Peter Anderson, Xiaodong He, Chris Buehler, Damien Teney, Mark Johnson, Stephen Gould, and Lei Zhang. Bottom-Up and Top-Down Attention for Image Captioning and Visual Question Answering. *arXiv preprint arXiv:1707.07998*, 2017.
- [3] Pablo Arbeláez, Jordi Pont-Tuset, Jonathan T Barron, Ferran Marques, and Jitendra Malik. Multiscale combinatorial grouping. In *IEEE conference on computer vision and pattern recognition*, pages 328–335, 2014.
- [4] Hedi Ben-younes, Rémi Cadene, Matthieu Cord, and Nicolas Thome. MUTAN: Multimodal Tucker Fusion for Visual Question Answering. In *IEEE International Conference on Computer Vision*, pages 2612–2620, 2017.
- [5] Kyunghyun Cho, Bart Van Merriënboer, Caglar Gulcehre, Dzmitry Bahdanau, Fethi Bougares, Holger Schwenk, and Yoshua Bengio. Learning Phrase Representations using RNN Encoder-Decoder for Statistical Machine Translation. In *2014 Conference on Empirical Methods in Natural Language Processing*, pages 1724–1734, 2014.
- [6] Akira Fukui, Dong Huk Park, Daylen Yang, Anna Rohrbach, Trevor Darrell, and Marcus Rohrbach. Multimodal Compact Bilinear Pooling for Visual Question Answering and Visual Grounding. *arXiv preprint arXiv:1606.01847*, 2016.
- [7] Ross Girshick. Fast r-cnn. In *IEEE International Conference on Computer Vision*, pages 1440–1448, 2015.
- [8] Yash Goyal, Tejas Khot, Douglas Summers-Stay, Dhruv Batra, and Devi Parikh. Making the V in VQA Matter: Elevating the Role of Image Understanding in Visual Question Answering. In *IEEE Conference on Computer Vision and Pattern Recognition*, 2017.
- [9] Kaiming He, Xiangyu Zhang, Shaoqing Ren, and Jian Sun. Deep Residual Learning for Image Recognition. In *IEEE Conference on Computer Vision and Pattern Recognition*, 2016.
- [10] Ryota Hinami and Shin’ichi Satoh. Query-Adaptive R-CNN for Open-Vocabulary Object Detection and Retrieval. *arXiv preprint arXiv:1711.09509*, 2017.
- [11] Ronghang Hu, Huazhe Xu, Marcus Rohrbach, Jiashi Feng, Kate Saenko, and Trevor Darrell. Natural language object retrieval. In *IEEE Computer Vision and Pattern Recognition*, pages 4555–4564, 2016.
- [12] Ilija Ilijevski and Jiashi Feng. A Simple Loss Function for Improving the Convergence and Accuracy of Visual Question Answering Models. 2017.
- [13] Max Jaderberg, Karen Simonyan, Andrew Zisserman, and Koray Kavukcuoglu. Spatial Transformer Networks. In *Advances in Neural Information Processing Systems 28*, pages 2008–2016, 2015.
- [14] Jin-Hwa Kim, Sang-Woo Lee, Donghyun Kwak, Min-Oh Heo, Jeonghee Kim, Jung-Woo Ha, and Byoung-Tak Zhang. Multimodal Residual Learning for Visual QA. In *Advances in Neural Information Processing Systems 29*, pages 361–369, 2016.
- [15] Jin-Hwa Kim, Kyoung Woon On, Woosang Lim, Jeonghee Kim, Jung-Woo Ha, and Byoung-Tak Zhang. Hadamard Product for Low-rank Bilinear Pooling. In *The 5th International Conference on Learning Representations*, 2017.
- [16] Diederik P. Kingma and Jimmy Ba. Adam: A Method for Stochastic Optimization. In *International Conference on Learning Representations*, 2015.
- [17] Ranjay Krishna, Yuke Zhu, Oliver Groth, Justin Johnson, Kenji Hata, Joshua Kravitz, Stephanie Chen, Yanis Kalantidis, Li-Jia Li, David A Shamma, Michael Bernstein, and Li Fei-Fei. Visual genome: Connecting language and vision using crowdsourced dense image annotations. *arXiv preprint arXiv:1602.07332*, 2016.
- [18] Jiasen Lu, Jianwei Yang, Dhruv Batra, and Devi Parikh. Hierarchical Question-Image Co-Attention for Visual Question Answering. *arXiv preprint arXiv:1606.00061*, 2016.
- [19] Vinod Nair and Geoffrey E Hinton. Rectified Linear Units Improve Restricted Boltzmann Machines. *27th International Conference on Machine Learning*, pages 807–814, 2010.
- [20] Hyeonseob Nam, Jung-Woo Ha, and Jeonghee Kim. Dual Attention Networks for Multimodal Reasoning and Matching. In *IEEE Conference on Computer Vision and Pattern Recognition*, 2016.
- [21] Jeffrey Pennington, Richard Socher, and Christopher D Manning. GloVe: Global Vectors for Word Representation. *Proceedings of the 2014 Conference on Empirical Methods in Natural Language Processing*, 2014.

- [22] Hamed Pirsiavash, Deva Ramanan, and Charles C. Fowlkes. Bilinear classifiers for visual recognition. In *Advances in Neural Information Processing Systems 22*, pages 1482–1490, 2009.
- [23] Bryan A. Plummer, Liwei Wang, Chris M. Cervantes, Juan C. Caicedo, Julia Hockenmaier, and Svetlana Lazebnik. Flickr30k Entities: Collecting Region-to-Phrase Correspondences for Richer Image-to-Sentence Models. *International Journal of Computer Vision*, 123:74–93, 2017.
- [24] Joseph Redmon and Ali Farhadi. YOLO9000: Better, Faster, Stronger. In *IEEE Computer Vision and Pattern Recognition*, 2017.
- [25] Shaoqing Ren, Kaiming He, Ross Girshick, and Jian Sun. Faster R-CNN: Towards Real-Time Object Detection with Region Proposal Networks. *IEEE Transactions on Pattern Analysis and Machine Intelligence*, 39(6), 2017.
- [26] Anna Rohrbach, Marcus Rohrbach, Ronghang Hu, Trevor Darrell, and Bernt Schiele. Grounding of textual phrases in images by reconstruction. In *European Conference on Computer Vision*, pages 817–834, 2016.
- [27] Tim Salimans and Diederik P. Kingma. Weight Normalization: A Simple Reparameterization to Accelerate Training of Deep Neural Networks. *arXiv preprint arXiv:1602.07868*, 2016.
- [28] Nitish Srivastava, Geoffrey E. Hinton, Alex Krizhevsky, Ilya Sutskever, and Ruslan Salakhutdinov. Dropout : A Simple Way to Prevent Neural Networks from Overfitting. *Journal of Machine Learning Research*, 15 (1):1929–1958, 2014.
- [29] Damien Teney, Peter Anderson, Xiaodong He, and Anton van den Hengel. Tips and Tricks for Visual Question Answering: Learnings from the 2017 Challenge. *arXiv preprint arXiv:1708.02711*, 2017.
- [30] Alexander Trott, Caiming Xiong, and Richard Socher. Interpretable Counting for Visual Question Answering. In *International Conference on Learning Representations*, 2018.
- [31] Andreas Veit, Michael J Wilber, and Serge Belongie. Residual Networks are Exponential Ensembles of Relatively Shallow Networks. In *Advances in Neural Information Processing Systems 29*, pages 550–558, 2016.
- [32] Liwei Wang, Yin Li, and Svetlana Lazebnik. Learning Deep Structure-Preserving Image-Text Embeddings. In *IEEE Conference on Computer Vision and Pattern Recognition*, pages 5005–5013, 2016.
- [33] Mingzhe Wang, Mahmoud Azab, Noriyuki Kojima, Rada Mihalcea, and Jia Deng. Structured Matching for Phrase Localization. In *European Conference on Computer Vision*, volume 9908, pages 696–711, 2016.
- [34] Peng Wang, Qi Wu, Chunhua Shen, and Anton van den Hengel. The VQA-Machine: Learning How to Use Existing Vision Algorithms to Answer New Questions. In *Computer Vision and Pattern Recognition (CVPR)*, pages 1173–1182, 2017.
- [35] Huijuan Xu and Kate Saenko. Ask, Attend and Answer: Exploring Question-Guided Spatial Attention for Visual Question Answering. In *European Conference on Computer Vision*, 2016.
- [36] Raymond A Yeh, Jinjun Xiong, Wen-Mei W Hwu, Minh N Do, and Alexander G Schwing. Interpretable and Globally Optimal Prediction for Textual Grounding using Image Concepts. In *Advances in Neural Information Processing Systems 30*, 2017.
- [37] Peter Young, Alice Lai, Micah Hodosh, and Julia Hockenmaier. From image descriptions to visual denotations: New similarity metrics for semantic inference over event descriptions. *Transactions of the Association for Computational Linguistics*, 2:67–78, 2014.
- [38] Zhou Yu, Jun Yu, Chenchao Xiang, Jianping Fan, and Dacheng Tao. Beyond Bilinear: Generalized Multi-modal Factorized High-order Pooling for Visual Question Answering. *IEEE Transactions on Neural Networks and Learning Systems*, 2018.
- [39] Jianming Zhang, Zhe Lin, Jonathan Brandt, Xiaohui Shen, and Stan Sclaroff. Top-Down Neural Attention by Excitation Backprop. In *European Conference on Computer Vision*, volume 9908, pages 543–559, 2016.
- [40] Yan Zhang, Jonathon Hare, and Adam Prügel-Bennett. Learning to Count Objects in Natural Images for Visual Question Answering. In *International Conference on Learning Representations*, 2018.
- [41] C Lawrence Zitnick and Piotr Dollár. Edge boxes: Locating object proposals from edges. In *European Conference on Computer Vision*, pages 391–405, 2014.

Bilinear Attention Networks — Appendix

A Variants of BAN

A.1 Enhancing glove word embedding

We augment a computed 300-dimensional word embedding to each 300-dimensional Glove word embedding. The computation is as follows: 1) we choose arbitrary two words w_i and w_j from each question can be found in VQA and Visual Genome datasets or each caption in MS COCO dataset. 2) we increase the value of $\mathbf{A}_{i,j}$ by one where $\mathbf{A} \in V' \times V'$ is an association matrix initialized with zeros. Notice that i and j can be the index out of vocabulary V and the size of vocabulary in this computation is denoted by V' . 3) to penalize highly frequent words, each row of \mathbf{A} is divided by the number of sentences (question or caption) which contain the corresponding word. 4) each row is normalized by the sum of all elements of each row. 5) we calculate $\mathbf{W}' = \mathbf{A} \cdot \mathbf{W}$ where $\mathbf{W} \in V' \times E$ is a Glove word embedding matrix and E is the size of word embedding, *i.e.*, 300. Therefore, $\mathbf{W}' \in V' \times E$ stands for the mixed word embeddings of semantically closed words. 6) finally, we select V rows from \mathbf{W}' corresponding to the vocabulary in our model and augment these rows to the previous word embeddings, which makes 600-dimensional word embeddings in total. The input size of GRU is increased to 600 to match with these word embeddings. These word embeddings are fine-tuned.

As a result, this variant significantly improves the performance to 66.03 (± 0.12) compared with the performance of 65.72 (± 0.11) which is done by augmenting the same 300-dimensional Glove word embeddings (so the number of parameters is controlled). In this experiment, we use four-glimpse BAN and evaluate on validation split. The standard deviation is calculated by three random initialized models and the means are reported. The result on test-dev split can be found in Table 3 as *BAN+Glove*.

A.2 Integrating counting module

The counting module [40] is proposed to improve the performance related to counting tasks. This module is a neural network component to get a dense representation from spatial information of detected objects, *i.e.*, the left-top and right-bottom positions of the ϕ proposed objects (rectangles) denoted by $\mathbf{S} \in \mathbb{R}^{4 \times \phi}$. The interface of the counting module is defined as:

$$\mathbf{c} = \text{Counter}(\mathbf{s}, \tilde{\alpha}) \quad (12)$$

where $\mathbf{c} \in \mathbb{R}^{\phi+1}$ and $\tilde{\alpha} \in \mathbb{R}^{\phi}$ is the logits of corresponding objects for sigmoid function inside the counting module. We found that the $\tilde{\alpha}$ defined by $\max_{j=1, \dots, \phi} (A_{\cdot, j})$, *i.e.*, the maximum values in each column vector of A in Equation 9, was better than that of summation. Since the counting module does not support variable-object inputs, we select 10-top objects for the input instead of ϕ objects based on the values of $\tilde{\alpha}$.

The BAN integrated with the counting module is defined as:

$$\mathbf{f}_{i+1} = (\text{BAN}_i(\mathbf{f}_i, \mathbf{Y}; \mathcal{A}_i) + g(\mathbf{c})) \cdot \mathbf{1}^T + \mathbf{f}_i \quad (13)$$

where the function $g(\cdot)$ is a linear embedding followed by ReLU activation function. Note that a dropout layer before this linear embedding severely hurts performance.

As a result, this variant significantly improves the counting performance from 54.92 (± 0.30) to 58.21 (± 0.49), while overall performance is improved from 65.81 (± 0.09) to 66.01 (± 0.14) in a controlled experiment using a vanilla four-glimpse BAN. The definition of a subset of counting questions comes from the previous work [30]. The result on test-dev split can be found in Table 3 as *BAN+Glove+Counter*, notice that, which is applied by the previous embedding variant, too.

A.3 Integrating multimodal factorized bilinear (MFB) pooling

Yu et al. [38] extend low-rank bilinear pooling [15] with the rank $\mathbf{k} > 1$ and two factorized three-dimensional matrices, which called as MFB. The implementation of MFB is effectively equivalent to low-rank bilinear pooling with the rank $d' = d \times \mathbf{k}$ followed by sum pooling with the window size of \mathbf{k} and the stride of \mathbf{k} , defined by $\text{SumPool}(\tilde{\mathbf{U}}^T \mathbf{x} \circ \tilde{\mathbf{V}}^T \mathbf{y}, \mathbf{k})$. Notice that a pooling matrix \mathbf{P} in Equation 2 is not used. The variant of BAN inspired by MFB is defined as:

$$\mathbf{z}_{k'} = \sigma(\mathbf{X}^T \tilde{\mathbf{U}})_{k'}^T \cdot \mathcal{A} \cdot \sigma(\mathbf{Y}^T \tilde{\mathbf{V}})_{k'} \tag{14}$$

$$\mathbf{f}' = \text{SumPool}(\mathbf{z}, \mathbf{k}) \tag{15}$$

where $\tilde{\mathbf{U}} \in \mathbb{R}^{N \times K'}$, $\tilde{\mathbf{V}} \in \mathbb{R}^{M \times K'}$, σ denotes ReLU activation function, and $\mathbf{k} = 5$ following Yu et al. [38]. Notice that $K' = K \times \mathbf{k}$ and k' is the index for the elements in $\mathbf{z} \in \mathbb{R}^{K'}$ in our notation.

However, this generalization was not effective for BAN. In Figure 2b, the performance of *BAN-I+MFB* is not significantly different from that of *BAN-I*. Furthermore, the larger K' increases the peak consumption of GPU memory which hinders to use multiple-glimpses for the BAN.

Table 5: Test-standard scores of ensemble-model on VQA 2.0 dataset to compare state-of-the-arts. Excerpt from the VQA 2.0 Leaderboard at the time of writing. # denotes the number of models for their ensemble method.

Team Name	#	Overall	Yes/no	Number	Other
vqateam_mcb_benchmark [6, 8]	1	62.27	78.82	38.28	53.36
vqa_hack3r	-	62.89	79.88	38.95	53.58
VQAMachine [34]	-	62.97	79.82	40.91	53.35
NWPU_VQA	-	63.00	80.38	40.32	53.07
yahia zakaria	-	63.57	79.77	40.53	54.75
ReasonNet_	-	64.61	78.86	41.98	57.39
JuneflowerIvaNlpr	-	65.70	81.09	41.56	57.83
UPMC-LIP6 [4]	-	65.71	82.07	41.06	57.12
Athena	-	66.67	82.88	43.17	57.95
Adelaide-Teney	-	66.73	83.71	43.77	57.20
LV_NUS [12]	-	66.77	81.89	46.29	58.30
vqahhi_drau	-	66.85	83.35	44.37	57.63
CFM-UESTC	-	67.02	83.69	45.17	57.52
VLC Southampton [40]	1	68.41	83.56	51.39	59.11
Tohoku CV	-	68.91	85.54	49.00	58.99
VQA-E	-	69.44	85.74	48.18	60.12
Adelaide-Teney ACRV MSR [29]	30	70.34	86.60	48.64	61.15
DeepSearch	-	70.40	86.21	48.82	61.58
HDU-USYD-UNCC [38]	8	70.92	86.65	51.13	61.75
BAN+Glove+Counter (ours)	1	70.35	85.82	53.71	60.69
BAN Ensemble (ours)	8	71.72	87.02	54.41	62.37
BAN Ensemble (ours)	15	71.84	87.22	54.37	62.45

Table 6: Recall@1 performance over types for Flickr30k Entities (%)

Model	People	Clothing	Body Parts	Animals	Vehicles	Instruments	Scene	Other
Rohrbach et al. [26]	60.24	39.16	14.34	64.48	67.50	38.27	59.17	30.56
Plummer et al. [23]	64.73	46.88	17.21	65.83	68.75	37.65	51.39	31.77
Yeh et al. [36]	68.71	46.83	19.50	70.07	73.75	39.50	60.38	32.45
Hinami and Satoh [10]	78.17	61.99	35.25	74.41	76.16	56.69	68.07	47.42
BAN (ours)	79.90	74.95	47.23	81.85	76.92	43.00	68.69	51.33
# of Instances	5,656	2,306	523	518	400	162	1,619	3,374